2014 IEEE International Conference on Robotics & Automation (ICRA)
Hong Kong Convention and Exhibition Center
May 31 - June 7, 2014. Hong Kong, China

Modeling the Dynamics of Perching with Opposed-Grip Mechanisms

Hao Jiang, Morgan T. Pope, Elliot W. Hawkes, David L. Christensen, Matthew A. Estrada, Andrew Parlier, Richie Tran, and Mark R. Cutkosky

***Abstract*— Perching allows Micro Aerial Vehicles (MAVs) avoid the power costs and electrical and acoustic noise of sustained flight, for long-term surveillance and reconnaissance applications. This paper presents a dynamic model that clarifies the requirements for repeatable perching on walls and ceilings using an opposed-grip mechanism and dry adhesive technology. The model predicts success for perching over a range of initial conditions. The model also predicts the conditions under which other directional attachment technologies, such as microspines, will succeed. Experiments conducted using a launching mechanism for a range of different landing conditions confirm the predictions of the model and provide insight into future design improvements that are possible by modifying a few key damping and stiffness parameters.**

I. Introduction

MAVs are lightweight, agile and low cost platforms for surveillance, reconnaissance, and environmental monitoring. Recent research has improved their flight performance through advances in sensing, navigation, and cooperative control [1]–[3]. Perching allows MAVs to transition from flight to a stable observation location, enabling long-term surveillance and reconnaissance.

Perching requires adhesion, which can be generated using magnets, sticky materials, suction, Velcro, etc.. These methods tend to require special surface materials, active actuation, or large attachment and detachment forces. For perching on smooth surfaces, previous work used sticky materials and gecko inspired adhesives [4]–[6]. Spines have also been used for soft materials (e.g. wood) or landing on rough surfaces such as cement walls or roofing shingles [7]–[9]. These mechanisms are not currently designed to adhere to inverted surfaces. Other grasping mechanisms such as passive, avian-inspired legs have been used to perch on pipes [10]. Previous MAV perching projects have developed dynamic models of perching with fixed-wing MAVs to compute envelopes of trajectory states leading to successful attachment, or "landing envelopes" [8,11].

Recently, a passive perching mechanism was developed which uses directional dry adhesives and a fast opposed-grip loading strategy to enable a MicroQuad MAV to perch on an inverted smooth surface with very low attachment and detachment effort, allowing many perching cycles [6]. This paper expands previous theoretical work to create a model for perching dynamics, and extends that model to inform design requirements for a mechanism using microspines. The model is validated through a series of experiments on MAVs perching on walls and ceilings with different initial conditions

All authors are with the Dept. of Mechanical Engineering, Stanford University, Stanford, CA 94305, USA jianghao@stanford.edu

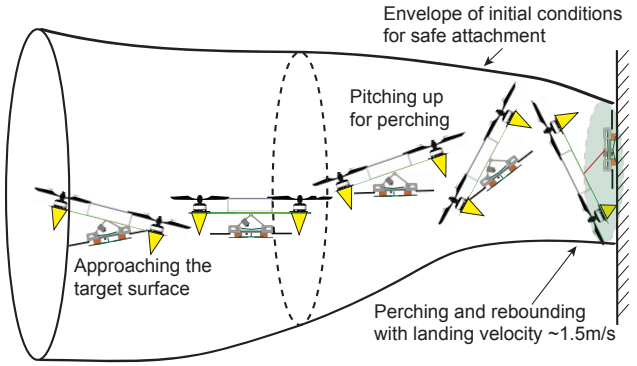

Fig. 1: Schematic of a landing envelope (funnel) of a quadrotor MAV perching on vertical surfaces with various initial conditions.

at touchdown. These conditions are assumed to be within the range of current MAV control systems (Fig. 1). Control strategies providing higher maneuverability could provide correspondingly higher perching success rates [7,12,13], but such work is not within the scope of this paper. Focusing on the implications of the validated model, we explore changes to damping and stiffness parameters of the mechanism that lead to an expanded envelope of initial conditions for which perching will succeed.

II. Dynamic Modeling of Perching Maneuver

As introduced in [6] and shown in Fig. 2, the perching mechanism is mounted under or above the MAV to save space and to facilitate wall and ceiling perching. This assumes that the MAV has the sensing and maneuverability necessary to detect a surface and orient the mechanism properly. Once in contact with the wall, the mechanism aligns itself with the surface and the velocity of the MAV forces a truss mechanism to collapse. As it does so, sliding joints (labeled (5) in Fig. 2) move apart and apply tension to the tile tendons. This action preloads the directional adhesive pads to turn them "on," and then locks the grip using a latch (4). The MAV rebounds from the surface, and a rebound spring (1), which connects the MAV to the gripping mechanism, stretches and absorbs the remaining energy. For detachment, a small actuator can release the latch.

This overall perching strategy can be divided into four phases: (1) mechanism alignment, (2) mechanism engagement, (3) collision and rebound, and (4) detachment. In subsequent sections we consider these phases in detail and conclude that a landing envelope can be estimated based primarily on (i) the damping during collision, (ii) energy

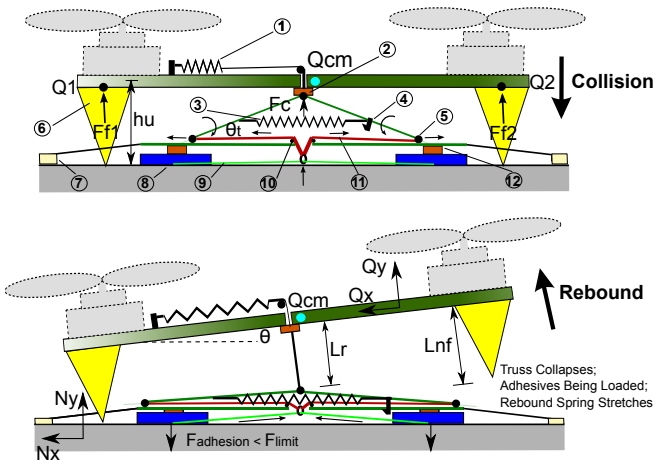

Fig. 2: Schematic of the perching gear and perching process. (1) Rebound Spring, (2) Compliant Foam Joint, (3) Truss Spring, (4) Latch, (5) Sliding Joint, (6) Damping Foam, (7) Outrigger, (8) Adhesive Tile, (9) Tile Tendon, (10) Pulley, (11) Truss Tendon, (12) Tile Supporting Foam.

.

absorbed in collapse, (iii) the adhesion limit surface of the attachment technology, and (iv) the rebound spring stiffness. Of these factors, only the adhesion limit surface is specific to the attachment technology. This result implies that other adhesive technologies with similar limit curves (e.g. spines) can be used to enable perching on different types of surfaces. The section concludes by defining the design constraints for opposed spine gripping on rough surfaces.

A. Mechanism Alignment

As discussed in [6], the perching mechanism must align with the surface before engagement begins. This can be accomplished reliably if: (1) the force applied to align the mechanism is less than the threshold force required to begin engagement, and (2) this aligning force acts to orient the mechanism before the adhesive tiles make contact.

B. Mechanism Engagement

The total energy absorption can be calculated based on truss spring stretch, sliding joint friction and pad foam compression:

$$\begin{aligned}\Delta E_k &= E_{spring} + E_{friction} \\ &= \frac{1}{2}k_{spring}(\Delta l_0^2 - \Delta l_1^2) + 2\mu \bar{f_n} l_{slide}\end{aligned} \tag{1}$$

where k_{spring} is the spring constant of the truss spring, Δl_0 and Δl_1 are the initial and final stretch of the truss spring, μ is the Coulomb friction coefficient of the sliding joint (≈ 0.2), $\bar{f_n}$ is the average normal force on the sliding joint ($\approx 0.4N$), and l_{slide} is the sliding range on one side of the truss ($3.7mm$). See also Fig. 2.

For the current landing gear design, the calculated energy absorption is ≈ 0.017 J. For a $120g$ micro-quadrotor with a typical landing velocity of approximately $1.7m/s$, this translates to $\approx 10\%$ of the total energy, and in isolation could reduce the velocity before collision by $\approx 5\%$.

Because the energy loss is small compared to the kinetic energy associated with a typical landing, the details of the force profile do not significantly affect the final landing envelope, as long as the force profile is smooth and the initial input force is larger than the self-alignment force [6]. If the shear component of the incoming velocity is too big compared to the normal component, the truss mechanism can jam and fail to grip (Fig. 3).[1] Reducing the truss angle θ_t enlarges the safe region.

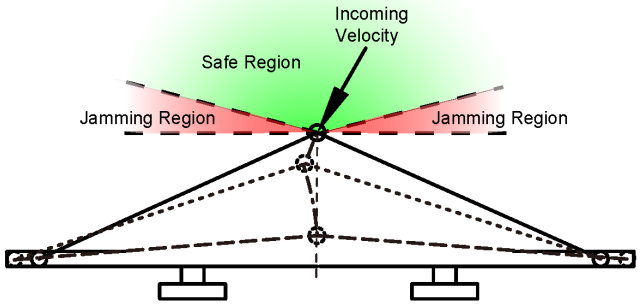

Fig. 3: Schematic of asymmetric truss collapse. The dotted line shows the truss sliding and impacting with one hard stop; the dashed line shows the truss fully collapsed; the dot-dashed line is the trajectory of the apex. When the incoming velocity is in the red region, the truss jams and fails to collapse. The green region indicates safe incoming velocities.

C. Collision and Rebound

Once the mechanism collapses, the quadrotor collides with the wall. This interaction is dominated by the foam attached to the quadrotor at the four distal points underneath each rotor and by the energy losses of collision. Assuming negligible lateral velocity lets us use a planar approximation, with the quadrotor represented as a single rigid body. The orientation of the quadrotor is chosen such that the upper and lower pairs of foam are modeled as single spring-dampers, and the wall is modeled as a very stiff spring-damper. To simulate the observed collision losses, we add a damping coefficient to the wall, approximating a coefficient of restitution of 0.25.

Once the vehicle bounces away from the wall and transitions to the rebound phase, the limit surface and the stiffness of the rebound spring are critical. As the MAV bounces away from the wall, forces are transmitted to the mechanism only through tension in the rebound spring. If this tension creates a force greater than the adhesion limit of the mechanism, failure occurs. The importance of damping in this analysis

[1] Additional asymmetric collapsing force results are shown at http://bdml.stanford.edu/Main/DynamicRotorcraftPerchingMechanisms.

motivated enlarging the foam dampers in comparison to an earlier design in [6].

D. Detachment

The magnetic latch is shown in Fig. 4. As the truss collapses, the hinge of the latch approaches the main board or chassis of the mechanism, causing a magnet to engage with another magnet below. The mechanism is then latched in place. The effort to unlatch the mechanism is low, ($40g$ force) and can be triggered by a small SMA actuator.

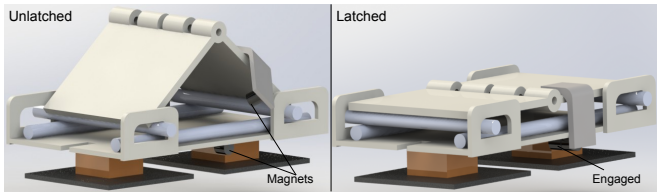

Fig. 4: Magnetic latch mechanism with low effort of engagement and disengagement.

E. Full Model For Envelope Prediction

We can now assemble a single model to predict perching success and failure. The details of aligning and engagement are well understood and can be neglected if we account for the total energy lost. This is accomplished by adding a single spring force between the wall and the quadrotor, activated only during engagement. The stiffness of this spring is tuned to absorb the amount of energy predicted by the analysis in Section II-B. The rest of the maneuver is dominated by the processes of collision and rebound as described above. The jamming forces caused by angles of impact close to θ_t (see II-B) restrict success to those initial conditions whose ratio of normal to tangential velocities is high enough to prevent jamming.

The dynamics of this engagement are governed by the following forces, each of which depends on certain conditions:

$$\begin{aligned}
F_C &= k_c(h_u - y_m)\hat{N}y && h_u > y_m > 0\\
&= 0 && else\\
F_{F1} &= -b_{fx}\dot{x}_{q1}\hat{N}x - b_f\dot{y}_{q1}\hat{N}y\\
&\quad + k_f(Ln_f - l_{f1})\hat{Q}y && l_{f1} < Ln_f\\
&= 0 && else\\
F_{F2} &= -b_{fx}\dot{x}_{q2}\hat{N}x - b_f\dot{y}_{q2}\hat{N}y\\
&\quad + k_f(Ln_f - l_{f2})\hat{Q}y && l_{f2} < Ln_f\\
&= 0 && else\\
F_{RS} &= -k_r l_r && y_{pads} = 0\\
&= 0 && else\\
F_W &= (-b_{wy}\dot{y_m} - k_w * y_m)\hat{N}y\\
&\quad + -b_{wx}\dot{x_m}\hat{N}x && y_m < 0\\
&= 0 && else
\end{aligned}$$

Identifier	Quantity	Range
Constants		
k_c	Collapsing Stiffness	$300N/m$
k_f, k_r, k_w	Stiffness of Foam, Rebound Spring and Wall	$85;150;10,000N/m$
b_f, b_w	Damping of Foam and Wall	$2.1;18Ns/m$;
h_u	Distance from cm to bottom of mechanism,	$0.312m$
L_{n_f}	Foam natural length	$.018m$
l_{f1}, l_{f2}	Length of first and second pair of foam dampers	$0 - L_{n_f}$
l_r	Deflection of rebound spring	$.05m$
Variables		
x_m, y_m	x and y of mechanism peak position	
x_{q1}, y_{q1}	x and y measure of first foam pair attachment point	
x_{q2}, y_{q2}	x and y measure of second foam pair attachment point	
y_{pads}	Current y measure of pad location	

TABLE I: Parameters and coordinates for simulation

where F_C is the force applied by the collapsing mechanism, F_{F1} and F_{F2} are the forces applied by the two pairs of foam respectively, F_{RS} is the force applied by the rebound spring, F_W is the force applied by the wall during collision, and the other identifiers correspond to those listed in Table I and illustrated in Fig. 2.

The forces produce three equations of motion to predict the motion of the MAV:

$$\begin{aligned}
m\ddot{y} = \quad & (F_C + F_{F1} + F_{F2} + F_{RS} + F_{Wall}) \cdot \hat{N}y\\
& -mg\sin(\phi) \qquad (2)\\
m\ddot{x} = \quad & (F_{F1} + F_{F2} + F_{RS} + F_{Wall}) \cdot \hat{N}x\\
& -mg_t\cos\phi \qquad (3)\\
I_{zz}\ddot{\theta} = \quad & [(Lq\hat{x} - hq\hat{y}) \times (F_{F1} - F_{F2}) +\\
& (-h_m q\hat{y}) \times (F_C + F_{Wall} + F_{RS})] \cdot \hat{N}z \qquad (4)
\end{aligned}$$

where ϕ is the angle of the landing surface relative to the ground.

The equations of motion are solved and numerically integrated forward in time, resulting in three possible results:

- If the MAV begins to move away from the wall without approaching closely enough for latching to occur, a failure is recorded.
- If latching is successful, pad failure can occur if the tension in the rebound spring exceeds the force necessary to peel engaged pads from the wall.
- If latching is successful and pad failure does not occur, the maneuver is predicted to succeed.

We can simulate over a range of trajectories to generate approximate landing envelopes. Section III compares the results of simulations with experiments.

F. Extension to Design Requirements for a Microspine Gripper

While dry adhesives work for smooth surfaces, spines are better for rough surfaces [8,14]. The model developed is agnostic to the adhesive technology, as long as it meets some broad design requirements. These requirements and a description of how they can be met by a microspine gripper are listed below.

1) *The adhesion capabilities of the technology should be expressible in terms of a limit surface.* This is satisfied for the choice of microspines [8,14].
2) *The mechanism must align to a surface before engagement begins.* This can be satisfied by a design with low rotational inertia and outriggers.
3) *The mechanism must reliably engage the adhesive when it is actuated.* The stochastic nature of asperity engagement means that spines must be dragged along the surface for approximately 1 cm to engage reliably. An enlarged version of the truss mechanism, which uses a large initial truss angle (θ_t) to achieve the required travel, is shown in Fig. 5.

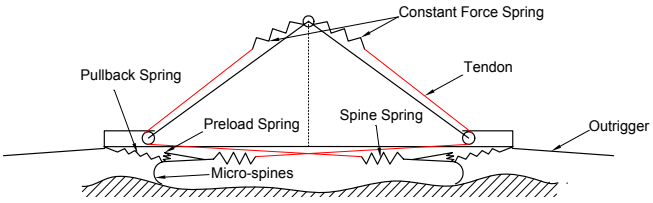

Fig. 5: Schematic of micro-spine mechanism.

III. Experimental Exploration and Verification

To verify the model, we designed an experiment to test perching success and failure over a subset of the possible trajectory space.

A. Experimental Setup

The test equipment consists of a launcher, a dummy MAV (of equivalent mass and similar mass distribution) outfitted with a dry adhesive perching mechanism, and a force/torque sensor. The launcher allows variation of tangential and normal velocities and angular misalignments for various landing surface orientations. Forces are measured at 1000 Hz using an ATI-Gamma SI-32-2.5 force/torque sensor and filtered using a zero-phase low-pass filter with cut-off frequency of 100 Hz to remove high-frequency noise.

B. Landing Force Verification

The force profiles for a series of successful attachments with normal velocities of ≈ 1.4 m/s and tangential velocities of ≈ 0.3 m/s were recorded and observed to remain within the empirical adhesion limit curve. These forces are plotted in Fig. 6, which also shows the profile of a typical landing failure with an incoming velocity of approximately 2.8 m/s. As shown in the figure, failure begins when the contact force reaches the bounds of the limit curve.

The force data were used to verify the parameters of the model and tune the parameters chosen for wall stiffness and damping. The resulting fit is shown in Fig. 7. The normal force fits well, and the simulation correctly predicts success and failure for the respective conditions. Fig. 8 shows the consistency of the force profile of five consecutive successful vertical surface landings.

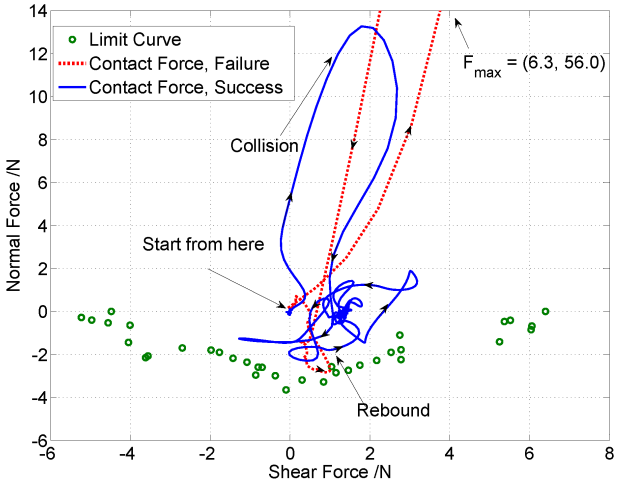

Fig. 6: Force profile for success and failure in perching on a vertical surface. Failure occurs as forces cross the limit curve, described by the green data points at the bottom of each figure. Forces for a successful landing remain above the limit curve. The limit curve corresponds to a pair of $2.25cm^2$ adhesive pads, where the maximum normal pressure is 8KPa (0.08 bar), and the largest shear stress is 14.4KPa (0.14 bar).

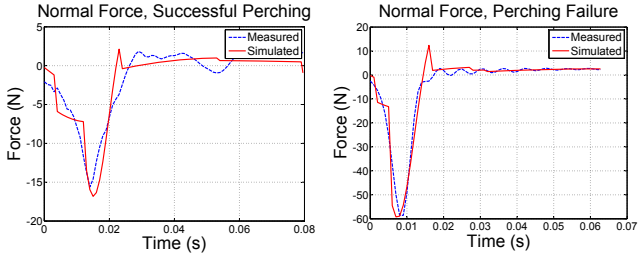

Fig. 7: Force profiles, simulation vs experiment, for the average of ten successful perches (left) and one perching failure (right)

C. Landing Envelope Verfication

Two common failure modes were observed. The first occurs when velocity is insufficient to engage the latch, and the second when the rebounding velocity is too high and exceeds the adhesive limit of the pads. A third failure mode was sometimes observed for high tangential velocities due to tangential displacement during pad contact. For the purpose of verifying the model, we focused on the two primary failure modes.

Landing envelope experiments utilized the same launcher as used for force profiles. Fig. 9 compares the results of the trials to predicted landing envelopes for three different configurations. These results confirm the general predictive ability of the model.

D. Microspine Gripper Performance

A microspine gripper was constructed and its limit surface generated by applying forces at various angles and recording the disengagement forces (Fig. 10). The gripper was tested for successful ballistic perching by throwing it

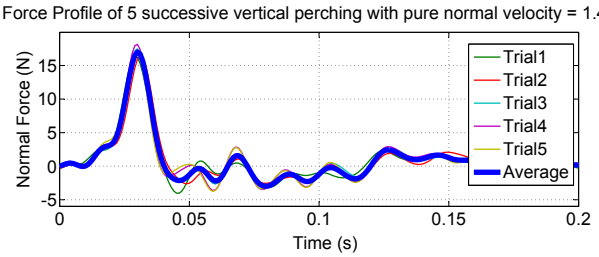

Fig. 8: Force profile of 5 consecutive successful vertical landings with $1.4m/s$ normal landing velocity.

at a vertical sheet of asphalt roofing shingle as shown in the accompanying video submission. When attached to the same simulated quadrotor body used for the dry adhesive verification experiments and launched with a normal velocity of $\approx 1.5m/s$ and a tangential velocity of $\approx 0.2m/s$, the device successfully perched in 17/20 trials.

IV. Findings

The models and experiments demonstrate that perching attachment can be predicted by a small set of parameters. Most important among these are the damping involved in collision, the limit surface of the mechanism, and the interaction between the rebound spring and the mechanism. Among these parameters, those which can be changed by the designer for a given perching mechanism are the damping coefficient of the foam attached to the quadrotor and the stiffness of the rebound spring. Together, they can be used to shape the landing envelope.

A. Damping

The amount of damping dramatically affects the behavior of the system, softening the collision and creates a lower rebound velocity. Increased damping results in an extension of the landing envelope as illustrated in Fig. 11. However, increased damping also detracts from the force required to engage the mechanism, and requires a higher inbound velocity to latch.

In the tangential direction, an increase in damping is beneficial as long as the attachment point of the foam does not induce large moments on the MAV. Indeed, a sufficiently high tangential damping coefficient can dramatically increase the landing envelope as shown in Fig. 11. A future design could tune the shape of the foam to increase tangential damping without changing the effects of damping in the normal direction.

While damping dissipates energy, an alternative solution for absorbing excess incoming kinetic energy is to store it as potential energy using the spring force of the attachment mechanism. For a single-point latch, this presents a similar increase in minimum velocity as that discussed for damping. A multi-point ratchet style like that described in [6] could reduce the lower velocity bound down to the resolution of the ratchet while retaining the option of storing excess energy for later use (for a jump-assisted takeoff).

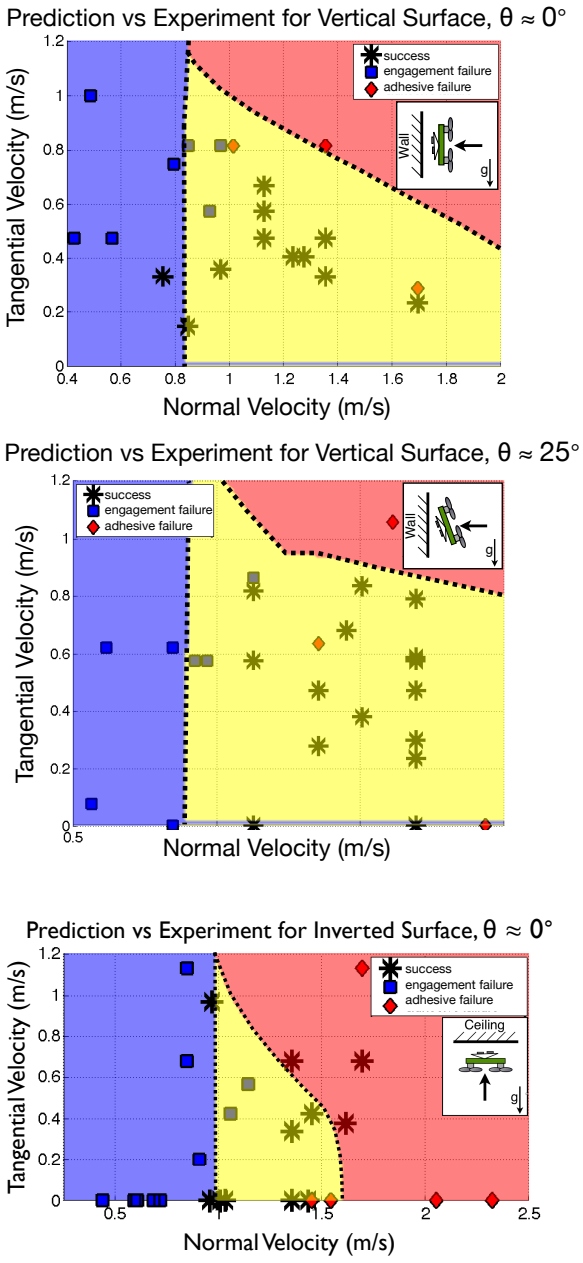

Fig. 9: Landing envelopes in velocity space for various configurations – vertical surface (top), vertical surface with 20° misalignment (middle), and inverted surface (bottom). The light red shading on right indicates predicted failure due to excessive rebound force, the blue central shading indicates predicted success, and the dark grey shading on left indicates predicted failure due to incomplete engagement.

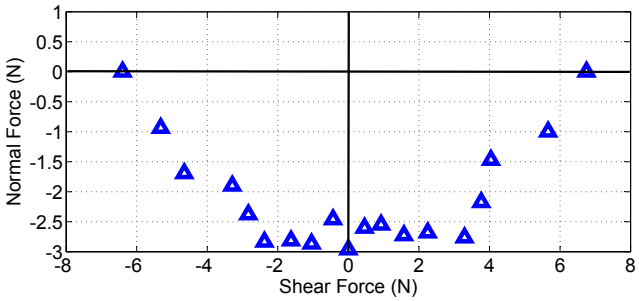

Fig. 10: Empirical limit curve for opposed microspine mechanism with two sets of 6 spines. Data are obtained by applying loads along different angles and recording failure forces.

B. Rebound Spring

Equally significant is the rebound spring. If no damping foam is used, the mechanism will engage with a minimum required normal velocity, but the resulting rebound will be violent. However, these force perturbations are only transmitted to the gripping device through the tension of the rebound spring. For a given rebound angle, the softer the rebound spring, the more work can be done by the spring on the rebounding robot before the force exceeds the adhesive limit. In theory, a soft enough rebound spring extends the landing envelope arbitrarily, although practical considerations prevent full realization of this ideal. Large landing envelopes might be obtained by removing damping (to allow for the lowest possible minimum velocity) and using a soft rebound spring to mitigate the resulting high rebound velocities. A predicted landing envelope for a system with no damping foam but a rebound spring of only one sixth the current rebound spring stiffness is shown in Fig. 11.

A superior design would also use a preloaded soft spring – or other approximation of a constant force spring – which could stretch to match the rebound energy with less deflection as discussed in [6].

V. CONCLUSIONS

We present a model of adhesive perching dynamics which informs design principles for robust MAV perching using opposed-grip mechanisms. For an appropriately designed mechanism, the model depends primarily on the interplay of energy absorption, adhesive limit surface, and rebound compensation. This insight is validated by experimental results, and a new microspine design demonstrates the extensibility of the results to a different adhesive technology intended for different surfaces. Future work includes designing mechanisms which realize some of the predicted performance improvements for any adhesive technology – for instance, changes in the damping foam and rebound spring systems. These insights and the new designs they motivate can help increase the incorporation of perching ability across a variety of new perching surfaces and MAV platforms.

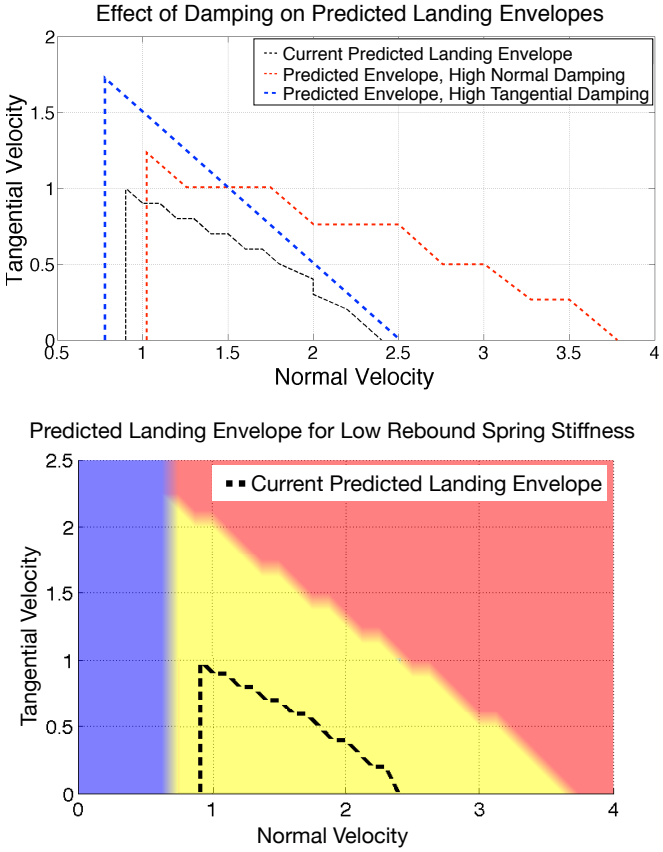

Fig. 11: Top: Changes in predicted landing envelope resulting from independently increasing the damping coefficient of the foam in normal and tangential directions by 2x and 4x, respectively. Bottom: Predicted landing envelope for system with $1/6$ rebound spring stiffness and no damping foam. Previous envelope shown by dashed line.

ACKNOWLEDGMENTS

Support for this work was provided by NSF IIS-1161679 and ARL MAST MCE 14-4 . The dynamic modeling for this paper was done using MotionGenesis software in consultation with Dr. Paul Mitiguy. E. Hawkes and M. Estrada are supported by NSF Graduate Fellowships.

REFERENCES

[1] D. Mellinger, N. Michael, and V. Kumar, "Trajectory generation and control for precise aggressive maneuvers with quadrotors," *The International Journal of Robotics Research*, vol. 31, no. 5, pp. 664–674, April 2012.

[2] M.W.Muller, M. Hehn, and R. D'Andrea, "Cooperative quadrocopter ball throwing and catching," in *IEEE International Conference on Intelligent Robot Systems*, 2012.

[3] A. M. Hyslop and J. S. Humbert, "Autonomous navigation in 3-d urban environments using wide-field integration of optic flow," *AIAA Journal of Guidance, Control, and Dynamics*, vol. 33, no. 1, pp. 147–159, 2010.

[4] M. L. Anderson, B. M. H. C. J. Perry, D. S. Olsen, J. R. Parcus, K. M. Pederson, , and D. D. Jensen, "The sticky-pad plane and other innovative concepts for perching uavs," in *47th AIAA Aerospace Sciences Meeting*, 2009.

[5] L. Daler, A. Klaptocz, A. Briod, M. Sitti, and D. Floreano, "A perching mechanism for flying robots using a fibre-based adhesive," in *IEEE International Conference on Robotics and Automation*, 2013.

[6] E. W. Hawkes, D. L. Christensen, E. V. Eason, M. A. Estrada, M. Heverly, E. Hilgemann, H. Jiang, M. T. Pope, A. Parness, and M. R. Cutkosky, "Dynamic surface grasping with directional adhesion," in *IEEE International Conference on Intelligent Robot Systems*, 2013.

[7] D. Mellinger, M. Shomin, and V. Kumar, "Control of quadrotors for robust perching and landing," in *in Proc. Int. Powered Lift Conf*, pp. 119–126, 2010.

[8] A. Lussier-Desbiens, A. T. Asbeck, and M. R. Cutkosky, "Landing, perching and taking off from vertical surfaces," *The International Journal of Robotics Research*, vol. 30, no. 3, pp. 355–370, 2011.

[9] M. Kovac, J. M. Germann, C. Hurzeler, R. Siegwart, and D. Floreano, "A perching mechanism for micro aerial vehicles," *Journal of Micro-Nano Mechatronics*, vol. 5, pp. 77–91, 2009.

[10] C. E. Doyle, J. J. Bird, T. A. Isom, J. C. Kallman, D. F. Bareiss, D. J. Dunlop, R. J. King, J. J. Abbott, and M. A. Minor, "An avian-inspired passive mechanism for quadrotor perching," *Mechatronics, IEEE/ASME Transactions on*, vol. 18, no. 2, pp. 506–517, 2013.

[11] E. Glassman, A. Lussier-Desbiens, M. Tobenkin, M. Cutkosky, and R. Tedrake, "Region of attraction estimation for a perching aircraft: A lyapunov method exploiting barrier certificates," *IEEE International Conference on Robotics and Automation*, 2012.

[12] J.W.Roberts and R.Tedrake, "On the controllability of fixed-wing perching," *American Control Conference*, 2009.

[13] A.A.Paranjape, S.J.Chung, and J.Kim., "Novel dihedral-based control of flapping-wing aircraft with application to perching," *IEEE Transactions on Robotics*, 2013.

[14] A.T.Asbeck and M.R.Cutkosky, "Designing compliant spine mechanisms for climbing," *ASME Journal of Mechanisms and Robotics*, vol. 4, no. 3, 2012.